J. Fluid Mech. (1999), *vol.* 379, *pp.* 255–277. Printed in the United Kingdom

Stability of viscoelastic shear flows subjected to steady or oscillatory transverse flow

By V. V. RAMANAN, K. A. KUMAR AND M. D. GRAHAM†

Department of Chemical Enginering and Rheology Research Center,
University of Wisconsin-Madison, Madison, WI 53706-1691, USA

(Received 11 May 1998 and in revised form 10 August 1998)

Experiments and theory show that hydrodynamic instabilities can arise during flow of viscoelastic liquids in curved geometries. A recent study has found that a relatively weak steady transverse flow can delay the onset of instability in the circular Couette geometry until the azimuthal Weissenberg number We_θ is significantly higher than without axial flow. In this work we investigate the effect of superposition of a time-periodic axial Couette flow on the viscoelastic circular Couette and Dean flow instabilities. The analysis, carried out for the upper-convected Maxwell and Oldroyd-B fluids, generally shows increased stability compared to when there is no axial flow. However, we also find that the system shows instability – synchronous resonance – for some values of the axial Weissenberg number, We_z and forcing frequency ω. In particular, instability can be induced not only when ω is of the order of the inverse relaxation time of the fluid but also when it is much smaller. Scaling arguments and numerical results indicate that the high-ω, low-We_z regime is essentially equivalent to $We_z = 0$ in the steady case, implying no stabilization. At high values of ω and We_z, scaling analysis shows that the flow will always be stable. Numerical results are in agreement with these conclusions. Consistent with previous results on parametrically forced systems, we find that the zero-frequency limit is singular. In this limit, the disturbances display quiescent intervals punctuated by periods of large transient growth and subsequent decay.

This study also presents linear and nonlinear stability results for the addition of steady axial Couette and Poiseuille flows to viscoelastic instabilities in azimuthal Dean flows. It is shown that, for high We_z, the qualitative effect of adding a steady axial flow is similar to that in the circular Couette geometry, with a linear relationship between the critical We_θ and We_z. For low We_z, we find that the flow is stabilized, unlike in the circular Couette flow where the critical value of We_θ decreases at low We_z. Further, weakly nonlinear analysis shows that the criticality of the bifurcation depends on the value of We_z and the solvent viscosity, S. Finally, we also show the presence of a codimension-2 Takens–Bogdanov bifurcation point in the linear stability curve of Dean flow. This point represents a transition from one mechanism of instability to another.

1. Introduction

The problem of stability and dynamics of viscoelastic liquids in curved geometries has attracted considerable interest in recent years. Larson, Shaqfeh & Muller (1990, referred to from here on as LSM) first performed theoretical and experimental

† Author to whom correspondence should be addressed: email graham@engr.wisc.edu.

analysis of hydrodynamic instabilities arising in flow of viscoelastic fluids in an annular gap between concentric cylinders. It was shown that this 'viscoelastic Taylor–Couette' (VETC) instability was a purely elastic effect arising even at negligible Reynolds number. The criterion for instability to occur is that $\epsilon^{1/2} We_\theta = O(1)$, where We_θ is the azimuthal Weissenberg number (ratio between material and flow time scales) and ϵ is the gap width, non-dimensionalized with respect to the radius of the cylinder. The scaling reflects how large We_θ must be for the azimuthal normal (hoop) stress to contribute to the leading-order radial momentum balance. The mechanism of destabilization proposed by LSM and later refined by Joo & Shaqfeh (1994) to include non-axisymmetric modes, was based on the coupling of stress perturbations to the base-state velocity gradient to produce an azimuthal normal stress that drives radial and transverse motions leading to the formation of cells. The analysis of LSM for the upper-convected Maxwell (UCM) and Oldroyd-B models showed that the instability occurs as a degenerate Hopf bifurcation with the exact wave structure to be determined from nonlinear analysis (Golubitsky, Schaeffer & Stewart 1985). Avgousti & Beris (1993) provide a detailed discussion of symmetry issues in the context of axisymmetric perturbations. Later works (Joo & Shaqfeh 1994; Sureshkumar, Beris & Avgousti 1994) using the Oldroyd-B fluid model have shown that in fact non-axisymmetric modes are the most dangerous, with nonlinear analysis (Sureshkumar *et al.* 1994) predicting subcritical bifurcation for these modes and supercritical bifurcation for axisymmetric ones. Further, Renardy *et al.* (1996) conducted a nonlinear analysis to study mode interactions arising from the introduction of inertia – and thus the classical Taylor–Couette instability – into the system. Computations (Northey, Armstrong & Brown 1992; Avgousti, Liu & Beris 1993; Avgousti & Beris 1993) and experiments (Shaqfeh, Muller & Larson 1992) have shown that finite gap effects tend to stabilize the flow.

Joo & Shaqfeh (1991, 1992) were the first to report elastic instabilities in azimuthal Dean (pressure-driven) flow. In contrast to the VETC case, the Dean flow instability occurs as a steady bifurcation, and the most dangerous disturbance is axisymmetric. The mechanism of instability involves coupling of base-state hoop stresses with velocity perturbations. Joo & Shaqfeh (1994) also perform an *a posteriori* energy analysis to elucidate the mechanism of the instability.

Experimental and theoretical evidence shows that purely elastic instabilities are common in flows with curved streamlines (Shaqfeh 1996), and McKinley, Pakdel & Öztekin (1996) have described a method for generalizing the instability criterion for various geometries. Given the importance of such flows in polymer processing operations such as adhesive coating and the severe limitations in operating conditions that these instabilities impose, it is of practical importance to come up with schemes that can be used to suppress them. A recent study by Graham (1998) has shown that the addition of a relatively weak transverse secondary flow results in significant stabilization of the VETC flow. Superposition of transverse motion increases the critical azimuthal Weissenberg number for instability and moves the most unstable mode to longer wavelengths. The increased stability is due to the additional axial normal stresses generated by the transverse flow, which increase the resistance to radial displacements. Furthermore, scaling analysis and computations show that non-axisymmetric disturbances are strongly suppressed. A nonlinear analysis was performed which showed that in the narrow gap limit, the VETC instability is subcritical for the UCM fluid. However, the addition of a transverse Poiseuille flow resulted in a supercritical bifurcation, indicating a stable solution past the bifurcation point, while with superposed Couette flow, the bifurcation remained subcritical. One

aspect of the current work is the extension of that analysis to study the effect of superposed steady axial motion on Dean flow instabilities. A linear and weakly nonlinear stability analysis is carried out that elucidates the stability characteristics when the transverse motion is imposed by means of an axial pressure drop or by motion of the inner cylinder. As will be shown in §4, the onset of instability is delayed by the addition of transverse flow. In particular, it is shown that at large axial shear rates, the critical value of $\epsilon^{1/2}We_\theta$ scales linearly with the axial shear rate, confirming that a relatively weak transverse flow results in increased stability. This is similar to the behaviour seen in the VETC flow.

Having established that the addition of steady axial flow does stabilize the VETC and Dean flows, we investigate the effect of time-periodic axial motion on these flows. With its characteristic relaxation time scales, a viscoelastic fluid might be expected to interact with the time scale of a parametric forcing, giving rise to interesting dynamical phenomena. The effect of adding an oscillatory transverse flow has been examined for Newtonian Taylor–Couette flows, with experiments (Weisberg, Kevrekidis & Smits 1997) and analysis (Hu & Kelly 1995; Marques & Lopez 1997) showing that modulated axial flow does result in stabilization of the classical Taylor–Couette instability. Furthermore, the superposition of transverse oscillatory motion in shear flows has recently been used in a novel rheometer design (Vermant *et al.* 1997). Clearly, flow stability in such an apparatus is a natural concern. The questions we seek to answer in this paper are: Does time-periodic axial flow result in stabilization of the viscoelastic system? If so, at what regimes of oscillation frequency and amplitude do we obtain stabilization? Does the external forcing result in resonant modes that are characteristic of parametrically excited systems?

We begin with the formulation of the problem for an Oldroyd-B fluid with the narrow gap approximation in §2. Section 3 describes the details of the linear stability analysis used in the study. The external modulation gives rise to time-dependent coefficients in the disturbance equations. Linear stability analysis of the time-dependent equations is performed using Floquet theory, which is implemented through an Arnoldi technique to determine the dominant Floquet multipliers. The Arnoldi scheme is coupled to a time integration routine for the viscoelastic equations of motion. Section 4 summarizes the results of the effect of steady axial flow and presents results from the effect of axial flow on the Dean flow instability. Finally, in §5 we show results from our time-dependent analysis. The linear stability results obtained numerically are compared with predictions from high- and low-frequency asymptotic analysis. We also investigate the singularity of the zero frequency limit which has been reported in the literature by Marques & Lopez (1997) for Newtonian Taylor–Couette flows.

2. Formulation

We consider the inertialess flow of a UCM or Oldroyd-B fluid in the annular region between infinitely long circular cylinders. We assume that the annulus is open, i.e. we do not impose a constraint on the net axial flow rate. The fluid has relaxation time λ; the polymer and solvent contributions to the viscosity are η_p and η_s respectively, with the ratio η_s/η_p denoted by S. For the Couette problem, the inner cylinder, with radius R_1 is rotating with angular velocity Ω while the outer cylinder, with radius R_2, is stationary. Dean flow kinematics are produced by holding both cylinders fixed and imposing an azimuthal pressure drop. Schematics of the circular Couette and Dean flow geometries are shown in figures 1 (*a*) and 1 (*b*) respectively.

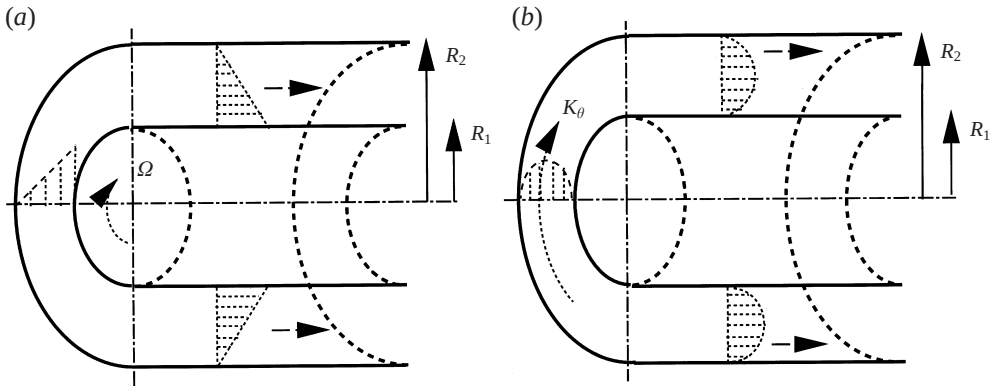

FIGURE 1. Schematic diagram of (*a*) the circular Couette (shown with an imposed axial Couette flow) and (*b*) Dean (shown with an imposed axial Poiseuille flow) geometries.

The dimensionless momentum, constitutive, and continuity equations are

$$\nabla \cdot \boldsymbol{\tau} - \nabla p + We_\theta S \nabla^2 \boldsymbol{v} = 0, \tag{2.1}$$

$$\boldsymbol{\tau} + We_\theta \left(\frac{\partial \boldsymbol{\tau}}{\partial t} + \boldsymbol{v} \cdot \nabla \boldsymbol{\tau} - \left(\boldsymbol{\tau} \cdot \nabla \boldsymbol{v} + (\boldsymbol{\tau} \cdot \nabla \boldsymbol{v})^{\mathrm{T}} \right) \right) = We_\theta \left(\nabla \boldsymbol{v} + \nabla \boldsymbol{v}^{\mathrm{T}} \right), \tag{2.2}$$

$$\nabla \cdot \boldsymbol{v} = 0, \tag{2.3}$$

where $\boldsymbol{v}$ is the velocity, p is the pressure and $\boldsymbol{\tau}$ is the polymer stress tensor. No-slip boundary conditions are imposed at the two cylinders. For Couette flow, the azimuthal Weissenberg number, We_θ, is defined by

$$We_\theta = \frac{\lambda \Omega (1 - \epsilon)}{\epsilon}, \tag{2.4}$$

where

$$\epsilon = \frac{R_2 - R_1}{R_2}, \tag{2.5}$$

and the corresponding definition for Dean flow in terms of the pressure drop $K_\theta = \partial P / \partial \theta$ is given by

$$We_\theta = -\frac{K_\theta \lambda \epsilon}{2 \eta_p}. \tag{2.6}$$

The Newtonian fluid is recovered for $S \to \infty$ with the pressure p rescaled accordingly. Note that $\epsilon/(1 - \epsilon)$ measures the maximum streamline curvature. Length is scaled with the gap width $R_2 - R_1 = \epsilon R_2$ and stress with η_p/λ. Velocity is scaled with the speed of inner cylinder rotation $(1 - \epsilon) R_2 \Omega$ for the Couette geometry and by $-K_\theta \epsilon^2 R_2 / 2\eta_p$ for the Dean geometry, which is the maximum shear rate times the length scale. Time is non-dimensionalized by $\epsilon R_2 / v^*$, where v^* is the velocity scale for the appropriate geometry. The dimensionless flow domain is $\{(r, \theta, z) : (1 - \epsilon)/\epsilon < r < 1/\epsilon, 0 < \theta \leqslant 2\pi, -\infty < z < \infty\}$. We also define a new radial coordinate, $\rho = r + 1 - 1/\epsilon$, so that $\rho = 0$ is the inner cylinder and $\rho = 1$ the outer.

Time-periodic axial Couette flow is imposed by moving the inner cylinder with

velocity $V\cos(\omega t)$, where V is the amplitude of the modulation and ω is the frequency which is scaled with $(1-\epsilon)\Omega/\epsilon$, the azimuthal shear rate. Axial flow introduces another dimensionless group, We_z, defined as

$$We_z = \frac{\lambda V(1-\epsilon)}{R_2\epsilon}. \tag{2.7}$$

At leading order in ϵ, i.e. in the narrow gap limit, $\omega = 0$ gives us the steady circular Couette with superimposed axial Couette flow (CCAC) discussed in Graham (1998), and the steady Dean flow with superposed axial Couette (DAC) flow presented later in this paper. When $\omega \neq 0$ we have the circular Couette with superimposed modulated axial Couette flow (CCMAC) and the Dean flow with superposed modulated axial Couette (DMAC) flow. Later in this paper we show that $\omega \to 0$ is a singular limit. We also show results for the Dean axial Poiseuille (DAP) flow where axial flow is due to a steady pressure gradient P_z in which case we redefine We_z to be

$$We_z = -\frac{P_z\,\lambda\epsilon R_2}{2\eta_p}. \tag{2.8}$$

For a UCM or Oldroyd-B fluid, one can find analytical expressions for the base-state velocities $\bar{\boldsymbol{v}}$ and polymer stresses $\bar{\boldsymbol{\tau}}$ in a circular Couette and Dean flow subjected to superposed time-periodic or steady axial flow. These expressions are shown in the Appendix. We are interested in the stability of these periodic solutions to infinitesimal perturbations. We define a vector of perturbations $\boldsymbol{u} = (\tilde{\tau}_{rr}, \tilde{\tau}_{r\theta}, \tilde{\tau}_{rz}, \tilde{\tau}_{\theta\theta}, \tilde{\tau}_{\theta z}, \tilde{\tau}_{zz}, \tilde{v}_r, \tilde{v}_\theta, \tilde{v}_z, \tilde{p})$, where, for example, $\tilde{\tau}_{\theta\theta} = \tau_{\theta\theta} - \bar{\tau}_{\theta\theta}$. It was shown by LSM for Couette flow and Joo & Shaqfeh (1991) for Dean flow that to recover the relevant regime for elastic instabilities, we must rescale the azimuthal Weissenberg number, We_θ to be $O(\epsilon^{-1/2})$. This is enforced by defining a new scaled Weissenberg number $Wp = \epsilon^{1/2}We_\theta$, which is $O(1)$ as $\epsilon \to 0$. Following LSM and Graham (1998), we also have the following scalings on the stresses and the velocities: $\tilde{\tau}_{rr} = O(1), \tilde{\tau}_{r\theta} = O(\epsilon^{-1/2}), \tilde{\tau}_{rz} = O(1), \tilde{\tau}_{\theta\theta} = O(\epsilon^{-1}), \tilde{\tau}_{\theta z} = O(\epsilon^{-1/2}), \tilde{\tau}_{zz} = O(1), \tilde{v}_r = O(\epsilon^{1/2}), \tilde{v}_\theta = O(1), \tilde{v}_z = O(\epsilon^{1/2}), \tilde{p} = O(1)$ and $We_z = O(1)$. This scaling can be inferred from the solution to the base-state stresses and velocities in the Appendix. In the equations with modulated axial forcing, a balance of terms is obtained by letting $\omega = \omega_1\epsilon^{1/2}$ and $t = t_1\epsilon^{-1/2}$ where ω_1 and t_1 are $O(1)$. With this scaling, the dimensionless relaxation time of the polymer is Wp. This is the 'low frequency' regime that includes all possible terms in the narrow gap approximation. Setting $\omega_1 = 0$ in this regime, we recover the steady equations of Graham (1998) for the CCAC and DAC flow equations shown later in this paper. We also investigate the effect of imposing a 'high frequency' oscillation by scaling ω to be an $O(1)$ quantity, i.e. we specify $\omega_1 = O(\epsilon^{-1/2})$. Dimensionally, this corresponds to a forcing frequency on the order of the azimuthal shear rate. In this regime the stability characteristics depend on the order of magnitude of the axial shear rate. In §5 we show that the relative magnitude of We_z with respect to ω_1 determines the appropriate balance of terms that affects the stability of the system. Asymptotic and numerical results are presented for both regimes later in this paper.

While this paper is concerned exclusively with elastic effects, we digress to comment on the relative scaling of the Reynolds number needed to include inertial effects in the formulation. In the narrow gap limit, the azimuthal Reynolds number, Re, must be $O(\epsilon^{-1/2})$ for the inertial terms to balance the divergence of the elastic stresses at leading order. Thus, small non-zero values of Reynolds number do not qualitatively change the results of the present analysis. The scaling regime $\epsilon^{1/2}Re = O(1)$ is where the classical (inertial) Taylor–Couette instability occurs.

3. Stability and numerical analysis

3.1. *Floquet theory and linear analysis*

To analyse the stability of the system we expand the perturbation vector using axisymmetric modes of the form

$$\boldsymbol{u} = \delta\phi(\rho, t)\mathrm{e}^{\mathrm{i}\alpha z} + O(\delta^2), \tag{3.1}$$

where $\phi = (\hat{\tau}_{rr}(\rho,t), \hat{\tau}_{r\theta}(\rho,t), \hat{\tau}_{rz}(\rho,t), \hat{\tau}_{\theta\theta}(\rho,t), \hat{\tau}_{\theta z}(\rho,t), \hat{\tau}_{zz}(\rho,t), \hat{v}_r(\rho,t), \hat{v}_\theta(\rho,t), \hat{v}_z(\rho,t))$ and α is the axial wavenumber, which is real and is specified. We emphasize that since it has been shown by Graham (1998) that in the steady case non-axisymmetric disturbances are strongly suppressed by axial flow, we restrict our analysis to axisymmetric modes. For linear stability analysis, these expansions are substituted in the governing equations and only first-order terms in δ are retained. We first consider the analysis of CCMAC and DMAC flows. Both flows are time periodic, and can hence be analysed using Floquet theory (Iooss & Joseph 1989). After applying spatial discretization, our problem has the form

$$\boldsymbol{E}\dot{\boldsymbol{u}} = \boldsymbol{A}(t)\boldsymbol{u}. \tag{3.2}$$

$\boldsymbol{A}(t)$ is a matrix with time-periodic coefficients such that $\boldsymbol{A}(t) = \boldsymbol{A}(t+T)$, where T is the period of the forcing function.† The solution $\boldsymbol{u}(T)$ at $t = T$, given the initial vector $\boldsymbol{u}(0)$, is

$$\boldsymbol{u}(T) = \Phi(T)\boldsymbol{u}(0), \tag{3.3}$$

where $\Phi(T)$ is the monodromy matrix, whose eigenvalues β, known as Floquet multipliers, determine the stability of the system. Stable and unstable behaviour are indicated by $|\beta| < 1$ and $|\beta| > 1$ respectively. The Floquet exponent σ is defined by the relation

$$\beta = \exp(\sigma T). \tag{3.4}$$

Suppose Ψ is an eigenvector of $\Phi(T)$ corresponding to the Floquet exponent σ. Then, it can be shown (Iooss & Joseph 1989) that the solution $\boldsymbol{w}(t)$ to $\boldsymbol{E}\dot{\boldsymbol{w}} = \boldsymbol{A}(t)\boldsymbol{w}$ with $\boldsymbol{w}(0) = \Psi$ has a T-periodic component $\zeta(t)$ given by

$$\boldsymbol{\zeta}(t) = \mathrm{e}^{-\sigma t}\boldsymbol{w}(t), \tag{3.5}$$

such that

$$\boldsymbol{\zeta}(t) = \boldsymbol{\zeta}(t+T). \tag{3.6}$$

Thus, the $\boldsymbol{\zeta}(t)$ corresponding to the dominant Floquet multiplier gives us information on the spatial structure and time evolution of the disturbance.

Our goal is to calculate the dominant eigenvalues β of the monodromy matrix Φ. We use a primitive variable formulation of the constitutive, momentum, and constitutive equations. Spatial discretization of the equations is carried out via a Chebyshev collocation technique that includes a staggered grid for the pressure to avoid the spurious modes that arise otherwise. Specifically, we use the Chebyshev–Gauss–Lobatto integration points for the velocities and stresses and the Chebyshev–Gauss points for pressure (Canuto *et al.* 1988) with 33 modes for velocities and stresses and 32 for pressure. This choice of spatial resolution is found to be adequate.

† The non-zero entries of $Wp\boldsymbol{A}(t)$ in equation 3.2 for the CCMAC and DMAC cases are available from the authors or the Journal of Fluid Mechanics Editorial Office.

Since our interest is restricted to picking out the dominant eigenvalues of $\Phi(T)$, we take recourse to the Arnoldi Method (Arnoldi 1951) to determine the critical eigenvalue. We use the public domain code ARPACK (Lehoucq, Sorensen & Yang 1997) to carry out the Arnoldi calculations. The advantage of the Arnoldi method lies in the fact that we do not need to explicitly construct $\Phi(T)$ in its entirety; we need only determine the action of the matrix on a vector, $\boldsymbol{q} \leftarrow \Phi(T)\boldsymbol{p}$. In our problem $\boldsymbol{q}$ is the solution vector obtained by integrating the time evolution equations for a given initial vector $\boldsymbol{p}$. The choice of the initial vector $\boldsymbol{p}$ is arbitrary, with the only requirement being that it satisfy the algebraic components of equation (3.2). In our case, this is ensured by choosing an arbitrary stress profile and solving the linear momentum and continuity equations for the corresponding velocities and pressure. To compute the periodic component $\zeta(t)$, we calculate the disturbance vector $\boldsymbol{w}(t)$ by integrating the time evolution equation (3.2) with initial conditions given by the eigenvector of the monodromy matrix obtained from ARPACK. This choice of starting value ensures that the periodicity condition given by equation (3.6) is not violated.

The integration of the time-dependent viscoelastic equations is performed using the EVSS decomposition (Rajagopalan, Armstrong & Brown 1990) of the total stress into elastic and viscous components, coupled with a fully implicit first-order time-stepping procedure. The time integration and eigenvalue routines were benchmarked against known eigenvalues for the steady case ($\omega = 0$) from Graham (1998) for CCAC flow and against the DAC results presented in this paper. In addition, the plane Couette flow limit was checked against the exact analytical results of Gorodtsov & Leonov (1967). Most calculations are performed with a time step $\Delta t = T/100$, while at very low frequencies we employ increased temporal resolution of $\Delta t = T/2500$. This high resolution is necessary to ensure the accuracy of the eigenvalue computation, which is checked by monitoring the periodicity of $\boldsymbol{\zeta}(t)$.

Next, we briefly discuss the linear stability analysis of DAC and DAP flows. The analysis closely follows the corresponding one for circular Couette flows in Graham (1998) and only an abbreviated version is presented below. The equations governing the evolution of perturbations to the base flow can be written succinctly as

$$\boldsymbol{E}\,\dot{\boldsymbol{u}} = \boldsymbol{L}\boldsymbol{u} + \boldsymbol{N}(\boldsymbol{u}), \tag{3.7}$$

where $\boldsymbol{L}$ is the linearization of the governing equations about the base flow, and $\boldsymbol{N}$ comprises the strictly nonlinear terms. In the analysis of the steady DAC and DAP flows, expansions (3.1) are written as

$$\boldsymbol{u} = \delta\phi(\rho)\mathrm{e}^{\mathrm{i}\alpha(z-ct)} + O(\delta^2), \tag{3.8}$$

where $c = c_r + \mathrm{i}\,c_i$ is the complex growth rate. This expression is substituted into equation (3.7). Retaining only terms linear in the amplitude δ and applying the narrow gap approximation yields a complex generalized eigenvalue problem for the growth rate c. For given values of α and We_z, the base solution loses stability at the value of Wp for which $c_i = 0$.

3.2. *Weakly nonlinear analysis*

Following the methodology of Graham (1998) which in turn follows Iooss & Joseph (1989), we conduct a weakly nonlinear analysis to determine the criticality of the bifurcation in DAC and DAP flows. In the presence of either type of axial flow, the loss of stability takes the form of a Hopf bifurcation, while in the absence of axial flow the bifurcation is a pitchfork. In either case, the vectors take the form

of complex conjugates, and since we are only interested in real-valued solutions, the analysis described below works whether or not an axial flow is present.

The nonlinear solutions are constructed by expanding all variables as a power series in the amplitude δ, substituting in equation (3.7), and applying the narrow gap approximation at each order. We let $\mu = Wp - Wp_c$, $\hat{\omega}_0 = -\alpha c_r$, and $s = \hat{\omega} t$. Thus, the solution takes the form

$$\begin{pmatrix} \boldsymbol{u}(z,s,\delta) \\ \mu(\delta) \\ \hat{\omega}(\delta) - \hat{\omega}_0 \end{pmatrix} = \sum_{k=1}^{\infty} \frac{\delta^k}{k!} \begin{pmatrix} \boldsymbol{u}_k(z,s) \\ \mu_k \\ \hat{\omega}_k \end{pmatrix}, \tag{3.9}$$

where $\boldsymbol{u}$ is taken to be the solution at the Chebyshev points. The linear operator $\boldsymbol{L}$ can be written as

$$\boldsymbol{L}(\mu) = \boldsymbol{L}_0 + \delta\mu_1 \boldsymbol{L}' + \frac{\delta^2}{2}\mu_2 \boldsymbol{L}'' + . \tag{3.10}$$

Further, we define the following inner products:

$$\langle a(z,s), b(z,s)\rangle \equiv \frac{\alpha}{4\pi^2} \int_0^{2\pi/\alpha} \int_0^{2\pi} a(z,s)\, \bar{b}(z,s)\, \mathrm{d}s\, \mathrm{d}z, \tag{3.11}$$

and

$$[a(z,s), b(z,s)] \equiv \sum_{l=0}^{9(N+1)+N-1} \langle a_l(z,s), b_l(z,s)\rangle. \tag{3.12}$$

At $O(\delta)$, we recover the linear stability problem, which has the real-valued solution $\boldsymbol{u}_1 = \boldsymbol{z} + \boldsymbol{z}^*$. Note that $\boldsymbol{u}$ is time-independent in the absence of axial flow, and a travelling wave otherwise. The eigenvectors are normalized so that $[\boldsymbol{z}, \bar{\boldsymbol{z}}] = 1$, where $\bar{\boldsymbol{z}}$ is the solution to the adjoint problem. A solvability condition at $O(\delta^2)$ gives

$$-2\mathrm{i}\,\hat{\omega}_1\, [\boldsymbol{E}\boldsymbol{u}_1, \boldsymbol{z}^*] + 2\mu_1 [\boldsymbol{L}'\boldsymbol{u}_1, \boldsymbol{z}^*] = -2\,[\boldsymbol{N}_2(\boldsymbol{u}), \boldsymbol{z}^*]. \tag{3.13}$$

The structure of the solutions at first order implies that the right-hand side of this equation vanishes. Upon separating the real and imaginary parts, the coefficient matrix of the resulting 2×2 real system has, in general, a non-vanishing determinant, and hence admits only the trivial solution for μ_1 and $\hat{\omega}_1$.

Substituting these values into the $O(\delta^2)$ problem, we see that the particular solution at that order can be written as

$$\boldsymbol{u}_2 = \boldsymbol{u}_{20} + \boldsymbol{u}_{22}\mathrm{e}^{2\mathrm{i}(\alpha z + s)} + \bar{\boldsymbol{u}}_{22}\mathrm{e}^{-2\mathrm{i}(\alpha z + s)}. \tag{3.14}$$

Here, $\boldsymbol{u}_{20}$ is given by

$$\boldsymbol{L}_{0,0}\boldsymbol{u}_{20} = -2\langle \boldsymbol{N}_2(\boldsymbol{u}), \boldsymbol{1}\rangle, \tag{3.15}$$

where $\boldsymbol{L}_{0,0}$ is obtained by replacing α by 0 in $\boldsymbol{L}_0$. The vector $\boldsymbol{u}_{22}$ is given by

$$(-2\mathrm{i}\hat{\omega}_0 \boldsymbol{E} + \boldsymbol{L}_{0,2\alpha})\boldsymbol{u}_{22} = -2\langle \boldsymbol{N}_2(\boldsymbol{u}), \boldsymbol{1}\mathrm{e}^{2\mathrm{i}(\alpha z + s)}\rangle, \tag{3.16}$$

where $\boldsymbol{L}_{0,2\alpha}$ is obtained by replacing α with 2α in $\boldsymbol{L}_0$. Unlike in Graham (1998), the present formulation retains pressure in the momentum equations. Hence, neither of the above equations is singular and the solution is obtained by LU decomposition. A solvability condition at $O(\delta^3)$ gives the single complex equation (or the 2×2 real system)

$$-\mathrm{i}\hat{\omega}_2 [\boldsymbol{E}\boldsymbol{u}_1, \boldsymbol{z}^*] + \mu_2 [\boldsymbol{L}'\boldsymbol{u}_1, \boldsymbol{z}^*] = -2[\boldsymbol{N}_3(\boldsymbol{u}), \boldsymbol{z}^*], \tag{3.17}$$

from which μ_2 and $\hat{\omega}_2$ can be obtained.

4. Effect of steady axial flow

In this section we recapitulate the results of Graham (1998) for the superposition of steady axial flow on circular Couette geometry (CCAC) and present results from a similar exercise to study the effect of axial flow on instabilities observed in the azimuthal Dean flow problem by Joo & Shaqfeh (1991). As mentioned in §3, the results presented in this paper consider only axisymmetric modes.

Analysis of the CCAC case indicates that the bifurcation is a subcritical Hopf. Low values of We_z result in destabilization, i.e. minimum critical values of Wp are lower than in the absence of axial flow, while at higher We_z significant stabilization is achieved. Let us denote by Wp_c the critical value of Wp at a given α and We_z. Let $Wp_{c,min}$ be the value of Wp_c at the global minimum of the neutral stability curve at a given We_z, and α_{min} the corresponding value of α. For $We_z \gg 1$, scaling analysis shows that $Wp_{c,min} = O(We_z)$, which is recovered numerically when $We_z \gtrsim 1$. This may be rewritten as $\epsilon^{1/2} We_\theta = O(We_z)$, which implies that for a given azimuthal Weissenberg number one needs to impose a relatively small axial flow rate to stabilize the flow. The inclusion of solvent viscosity S has an overall stabilizing effect, shifting the neutral curves upwards while having no effect on the scaling result.

We now present results from a linear stability analysis for the DAC and DAP flows. As reported by Joo & Shaqfeh (1994), axisymmetric modes are the most unstable in Dean flow, and our calculations indicate that this behaviour persists when axial flow is added. For the sake of brevity, we only present the results for axisymmetric modes and zero solvent viscosity. These are shown in figure 2 (*a*) for DAC flow and figure 2 (*b*) for DAP flow at high α. In contrast to the CCAC and CCAP cases, stabilization occurs for *all* values of We_z. Figure 3 shows a plot of $Wp_{c,min}$ vs. We_z for both DAC and DAP flows. The linear scaling of $Wp_{c,min}$ with We_z at high axial shear rates is evident. Non-zero solvent viscosity has a stabilizing effect, shifting the neutral curves upward, while decreasing the critical wavenumber. This is similar to the behaviour observed at $We_z = 0$ by Joo & Shaqfeh (1992). Finally, figure 4 shows the neutral stability curve for pure Dean flow. We point out that there is a change in the slope of the curve at $\alpha = 21.9$, where the bifurcation changes from a pitchfork to a Hopf. This is a codimension-2 Takens–Bogdanov bifurcation point (Takens 1974; Bogdanov 1975; Knobloch & Proctor 1981; Guckenheimer & Knobloch 1983). Hereafter, we refer to this value of α as α_{tk}. For wavenumbers greater than α_{tk}, the bifurcation is a Hopf, with a four-dimensional centre manifold, similar to the one in circular Couette flow. As we decrease α towards α_{tk}, the period of the Hopf bifurcation increases, reaching infinity at α_{tk}, where the form of the bifurcation changes to a pitchfork. From a physical point of view, this bifurcation point is expected, since large-wavenumber disturbances are localized in a small region near the outer cylinder, and hence experience a base velocity profile that is locally linear, similar to the profile in circular Couette flow. Thus, we expect that for large wavenumbers, the destabilization mechanism, and hence the nature of the bifurcation, will be similar to the one in circular Couette flow.

Recent experimental results by Genieser (1997) on the flow of viscoelastic fluids through a planar contraction display instabilities that occur as transitions from steady flow to either steady or oscillatory flow, depending on contraction ratio. The oscillatory flows have very low frequency, so it may be that these observations are another manifestation of Takens–Bogdanov bifurcation and concomitant change in destabilization mechanism found here. The unfolding of a Takens–Bogdanov bifurcation in an $O(2)$ symmetric system (i.e. a system with axial translation and reflection symmetry, such as the one we have here) was performed by Dangelmayr

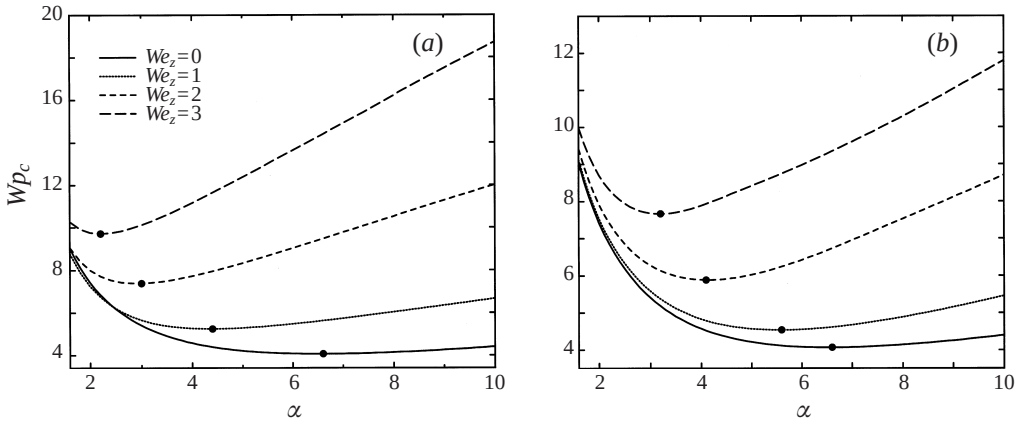

FIGURE 2. Neutral curve for (*a*) DAC and (*b*) DAP flow for varying We_z. $Wp_{c,min}$ is marked by a • for each case.

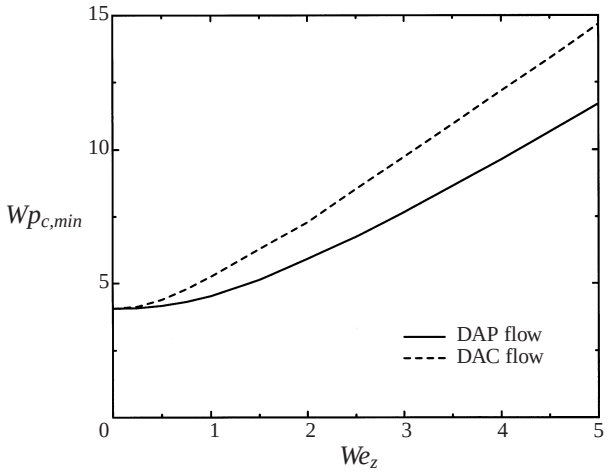

FIGURE 3. Plot of $Wp_{c,min}$ vs. We_z for DAC and DAP flows.

& Knobloch (1987). They showed that, depending on the value of the bifurcation parameters, observable patterns include a non-trivial steady state, travelling waves, standing waves and modulated waves.

The results of the weakly nonlinear analysis at $Wp_{c,min}$ and α_{min} are summarized in table 1 for DAC flow and table 2 for DAP flow. Negative values of μ_2 indicate subcritical behaviour while positive values imply supercriticality. We note that in the absence of solvent viscosity, $S = 0$, the bifurcation changes from subcritical to supercritical at $We_z \approx 0.05$ while at finite solvent viscosity the change occurs at $We_z \approx 1$. Results for higher We_z show that for $S \neq 0$ the bifurcations revert back to being subcritical. Clearly, by varying the extent of axial motion we may not only change the position of the bifurcation point but also ensure that we stay in a regime that admits stable solutions. Similar behaviour arises for the DAP flow, where there is a change in the sign of μ_2 at $We_z \approx 0.25$ for $S = 0$, and $We_z \approx 1.0$ when $S = 1$. Here, however, non-zero S does not change the criticality of the dominant unstable

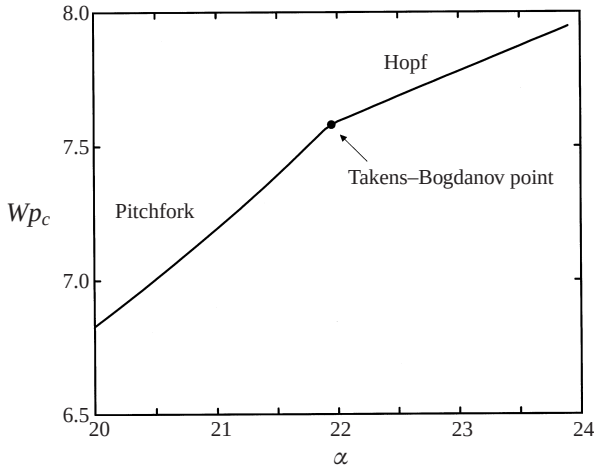

FIGURE 4. Neutral curve for DAC flow at high α. The change in slope at $\alpha_{tk} = 21.9$ indicates the Takens–Bogdanov bifurcation.

$S = 0$					$S = 1$				
We_z	α_{min}	$Wp_{c,min}$	μ_2	$\hat{\omega}_2$	We_z	α_{min}	$Wp_{c,min}$	μ_2	$\hat{\omega}_2$
0	6.6	4.06	−11.21	0	0	6.3	5.88	−484.67	0
0.05	6.6	4.07	−6.91	−0.74	1.0	4.8	7.03	−38.17	−2.58
0.1	6.5	4.07	0.27	−0.58	2.0	3.6	9.36	144.25	0.40
1.0	4.4	5.25	7.05	−0.48	3.0	3.0	11.81	123.18	4.15
2.0	2.9	7.39	26.92	−0.42	4.0	2.6	14.28	−145.25	4.77
3.0	2.2	9.73	46.21	0.24	5.0	2.3	16.76	−528.80	3.69
4.0	1.8	12.18	52.65	0.57					
5.0	1.5	14.68	54.15	0.66					

TABLE 1. μ_2 and $\hat{\omega}_2$ for DAC flow for $S = 0$ and $S = 1$.

mode at higher values of We_z. We note that a change in the criticality of bifurcation has also been observed in the weakly nonlinear analysis of cone-and-plate flow of an Oldroyd-B fluid (Olagunju 1997).

5. Effect of modulated axial flow

Our goal here is to investigate whether the addition of a periodic transverse flow will result in stabilization or destabilization of the primary azimuthal flow. From the Appendix, we observe that the expression for the steady-state axial stress $\bar{\tau}_{zz}$ is the sum of a constant $O(We_z^2)$ contribution and a periodic component. We know from Graham (1998) that the stabilization when the axial flow is steady is due to the We_z^2 term (refer to Graham (1998) for details of the stabilization mechanism) and in our problem the additional time-varying component can serve to strengthen or weaken the stabilizing effect leading to a stable or an unstable system. We observe both characteristics depending on the amplitude, We_z, and frequency, ω of the deformation rate. To study the transitions in stability arising from the variation of We_z and ω,

$S = 0$					$S = 1$				
We_z	α_{min}	$Wp_{c,min}$	μ_2	$\hat{\omega}_2$	We_z	α_{min}	$Wp_{c,min}$	μ_2	$\hat{\omega}_2$
0	6.6	4.06	−11.21	0	0	6.3	5.88	−484.67	0
0.2	6.5	4.08	−3.95	−0.42	1.0	5.7	6.42	−95.63	− 1.35
0.3	6.5	4.10	2.20	−0.14	2.0	4.5	7.92	151.33	− 1.20
1.0	5.6	4.54	7.73	−0.38	3.0	3.7	9.89	459.44	7.99
2.0	4.1	5.91	22.55	−2.05	4.0	3.2	11.99	717.29	19.51
3.0	3.2	7.60	40.10	−3.65	5.0	2.8	14.24	813.98	25.62
4.0	2.6	9.63	47.64	−2.83					
5.0	2.1	11.70	20.18	0.46					

TABLE 2. μ_2 and $\hat{\omega}_2$ for DAP flow for $S = 0$ and $S = 1$.

we use a combination of scaling and numerical analysis. Unless otherwise stated, all analysis presented here implicitly assumes that the solvent viscosity $S = 0$. Non-zero solvent viscosity does not change the conclusions of the asymptotic analysis and has no qualitative effect on the numerical results.

5.1. *Scaling analysis*

We begin by examining the results from a high-ω asymptotic analysis of the model equations. The results of such an analysis are invariant to whether the flow kinematics are governed by CCMAC or DMAC geometry.

To gain insight into the stability characteristics of the system at high frequency, we scale ω_1 to be $O(\epsilon^{-1/2})$ with the time variable rescaled appropriately to reflect the shorter time scales. Further, we also retain the scalings on the axial and azimuthal wavenumbers $We_z = Wp = O(1)$ and restrict α to be $O(1)$. In this regime, the axial strain rate is large, but the strain amplitude is small ($O(\epsilon^{1/2})$), and we find that the leading-order evolution equation for $\tilde{\tau}_{zz}$ does not contain the We_z^2 contribution that has been established to be the source of high normal axial stresses that contribute to the stabilization in the flow. The We_z^2 term comes from the time-averaged non-zero base-state axial stress (refer to the Appendix for $\bar{\tau}_{zz}$), which tends to zero with increasing ω and fixed We_z. Thus, we expect decreased stabilization in this regime. Further, the $\omega_1 = O(\epsilon^{-1/2})$ regime also lets us apply the method of averaging, a rigorous asymptotic technique (Sanders & Verhulst 1985), to the time-dependent equations. Briefly, the averaging method transforms the system

$$\dot{\boldsymbol{x}} = \hat{\epsilon}\boldsymbol{f}(\boldsymbol{x}, t, \hat{\epsilon}) \quad \text{with} \quad \boldsymbol{f}(\boldsymbol{x}, t, \hat{\epsilon}) = \boldsymbol{f}(\boldsymbol{x}, t + T, \hat{\epsilon}), \tag{5.1}$$

to an autonomous system

$$\dot{\boldsymbol{y}} = \hat{\epsilon}\frac{1}{T}\int_0^T \boldsymbol{f}(\boldsymbol{y}, t, 0)\,\mathrm{d}t = \hat{\epsilon}\bar{\boldsymbol{f}}(\boldsymbol{y}). \tag{5.2}$$

In other words, the averaging procedure replaces the time-dependent coefficients with their averages over the period of oscillation. This procedure is valid for arbitrary amplitude of oscillation as long as $\hat{\epsilon} \ll 1$. It can be shown that in our problem the equations governing the stress perturbations in this regime are of the form shown in equation (5.1) with $\hat{\epsilon} = \epsilon^{1/2}$, ϵ being the dimensionless gap width defined by equation (2.5). Importantly, we note the absence of the contribution due to the zero-frequency terms in $\bar{\tau}_{zz}$ in the leading-order equations for $\tilde{\tau}_{rz}$ and $\tilde{\tau}_{zz}$. The remaining coefficients

of We_z are periodic with zero mean and drop out in the averaging procedure, leaving a system that is independent of We_z and ω_1. Hence in the $\omega_1 = O(\epsilon^{-1/2})$ and $We_z = O(1)$ regime, the system is reduced to the steady circular Couette or Dean flow limit with no axial motion. Computational results presented later in this section corroborate this prediction.

In the second high-frequency regime of interest we investigate the effect of $O(1)$ axial deformation on the dynamics of the system. In this regime we have $\omega_1 = O(\epsilon^{-1/2})$ and $We_z = O(\epsilon^{-1/2})$. By considering time scales of the order of the relaxation time of the fluid, we discover the presence of stress boundary layers near the cylinders of size $O(1/We_z)$ for $O(1)$ wavenumbers and of size $O(1/\alpha We_z)$ for $O(\epsilon^{-1/2})$ wavenumbers. The existence of boundary layers at high shear rates is consistent with the analysis of Graham (1998) and Renardy (1997). The asymptotic balances reveal that the destabilizing azimuthal stress, $\tilde{\tau}_{\theta\theta}$, drops out of the radial momentum balance in both CCMAC and DMAC flows. The propagation of the purely elastic instability of viscoelastic liquids in curved geometries is through the development of an unstable stratification of the hoop stress. The absence of this contribution in the asymptotic limit points to a stable flow. Again, computational results confirm this prediction.

5.2. *Numerical analysis*

The numerical results are based on perturbation equations for $\omega_1 = O(1)$ and $We_z = O(1)$ with the remaining variables and parameters scaled as shown in §2. As discussed there, this frequency regime includes all possible terms in the narrow gap approximation, with $\omega_1 = 0$ reducing identically to the steady equations of Graham (1998). For most of our simulations, we choose $S = 0$ and $Wp = 5.93$ for CCMAC flow and $Wp = 4.06$ for the DMAC flow. These are the minimum critical values of Wp for the UCM fluid in the absence of axial flow. The presence of solvent viscosity has no qualitative effect on the results. The results in this section also serve to benchmark our numerical implementation against analytical results presented above. In our computations we vary ω_1 from 0.005 to 5.0 and We_z from 0.1 to 4.0. We find that this range of parameters is sufficient to capture the salient features and confirm predictions from asymptotic analyses of different frequency regimes. As stated previously, we restrict our analysis to axisymmetric modes with axial wavenumbers, α, varying from 2.0 to 9.0.

Figures 5(*a*)–5(*d*) summarize the stability information at various ω_1 and α for $Wp = 5.93$, $S = 0$, and $We_z = 1.0, 1.5, 2.0$ and 2.5 respectively in the CCMAC case. Computations are carried out for each marked point, which specifies ω_1 and α, and the result is shown by a $\circ$ if the dominant Floquet multiplier has magnitude less than unity indicating stability and a $\blacktriangle$ otherwise. Results for $We_z = 0.1$, $We_z = 3.0$ and $We_z = 4.0$ are not shown here since at these values Floquet analysis yields stability for all wavenumbers and frequencies. The plots show that at any specified axial shear rate one can find oscillation frequencies ω_1 where the flow is stabilized for all wavenumbers that we have considered. This establishes the fact that periodic forcing can be used to stabilize the flow. Indeed, we note that low forcing amplitudes ($We_z < 1$) that were shown to be destabilizing for the steady case can now have a stabilizing effect by judicious choice of the excitation frequency. In particular, we draw attention to $We_z = 0.1$ which shows stability at all ω_1 and α in contrast to steady results of Graham (1998), which predict $We_z = 0.1$ to be *destabilizing*. The stabilization is illustrated in figure 6(*a*) which shows the evolution of the norm of $\tilde{\tau}_{\theta\theta}$ for $We_z = 1.0$, $\alpha = 4.0$, and $\omega_1 = 0.383$ for CCMAC flow while figure 6(*b*) shows the same information for DMAC flow at $\omega_1 = 0.5$. In both these cases the initial

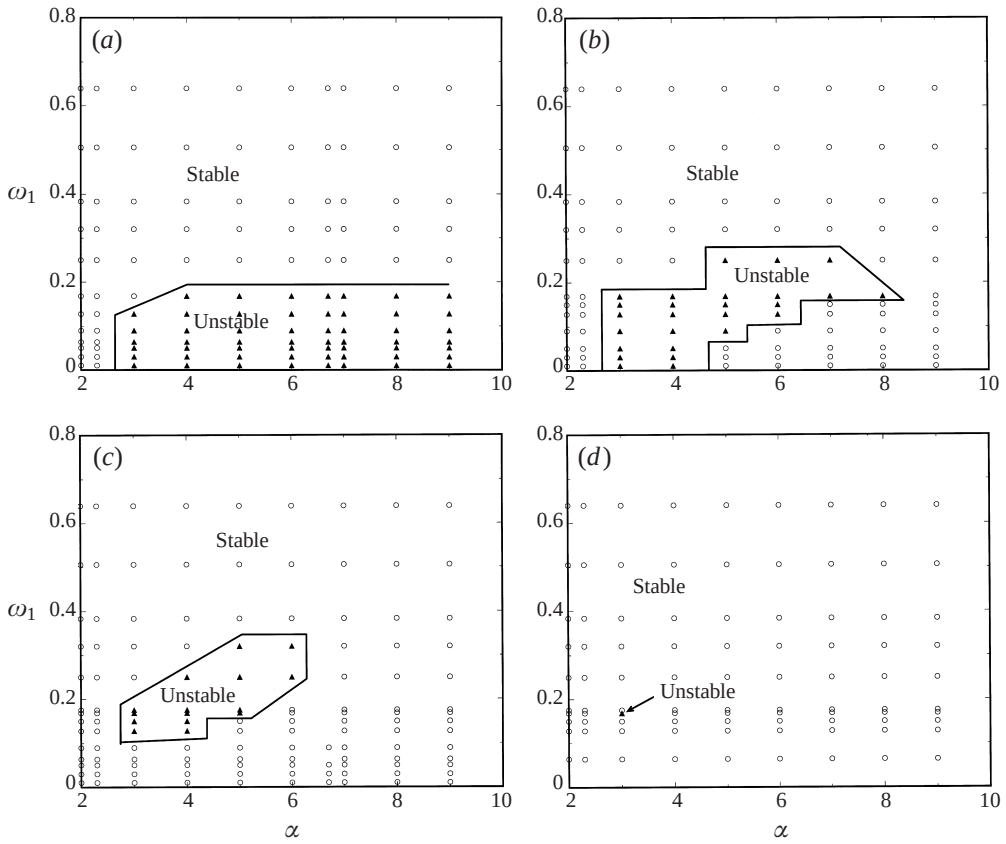

FIGURE 5. Stability maps for $Wp = 5.93$, varying We_z, ω_1, and α: (*a*) $We_z = 1.0$, (*b*) $We_z = 1.5$, (*c*) $We_z = 2.0$, (*d*) $We_z = 2.5$. Calculations for $We_z = 0.1$, $We_z = 3.0$ and $We_z = 4.0$ are not shown here since $|\beta| < 1$ for all wavenumbers and frequencies considered in this work.

condition for the time evolution is chosen to be the eigenvector at criticality in the absence of axial flow. Observe that the perturbation in the CCMAC case oscillates about the decaying exponential, consistent with the fact that the VETC instability occurs as a Hopf bifurcation, whereas the corresponding plot for DMAC flow shows a steady decay, which agrees with the analysis that the elastic instability in pure Dean flow takes the form of a pitchfork. We note further that for $\omega_1 > 0.5$ stabilization is achieved at all We_z. For these ω_1, plotting values of $|\beta|$ vs. ω_1 (in figure 7) for $\alpha = 6.7$ and varying We_z we find that the magnitude of the critical Floquet multiplier asymptotes to unity (i.e. to marginal stability) with increasing ω_1. This is consistent with our asymptotic analysis that predicts the recovery of the pure circular Couette limit in the $\omega_1 = O(\epsilon^{-1/2})$, $We_z = O(1)$ regime. Likewise, for higher We_z the stable Floquet multipliers are consistent with the $\omega_1 = O(\epsilon^{-1/2})$, $We_z = O(\epsilon^{-1/2})$ asymptotics that predict complete stabilization. In fact for $We_z > 2.5$ we find stability for all frequencies and wavenumbers that have been investigated. The stabilization trend is even stronger in the DMAC flow where we have found stabilization ($|\beta| < 1$) for all We_z, ω_1, and α that we have considered. As in the CCMAC case, the asymptotic predictions are corroborated by the numerical results.

Although complete stabilization occurs at some frequencies, there are clearly non-trivial regions where the oscillation destabilizes the CCMAC flow. These can be seen

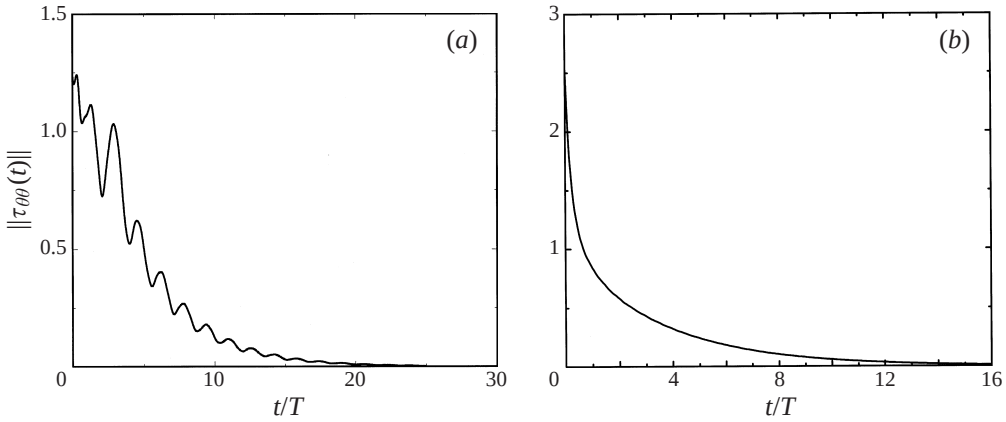

FIGURE 6. Norm of $\tilde{\tau}_{\theta\theta}$ vs. t/T (*a*) CCMAC flow with $Wp = 5.93$, $We_z = 1.0$, $\omega_1 = 0.383$, $\alpha = 6.7$. The disturbance decays in approximately 25 periods of oscillation. (*b*) DMAC flow with $Wp = 4.06$, $We_z = 1.0$, $\omega_1 = 0.5$, $\alpha = 6.6$. The disturbance decays in approximately 15 periods of oscillation.

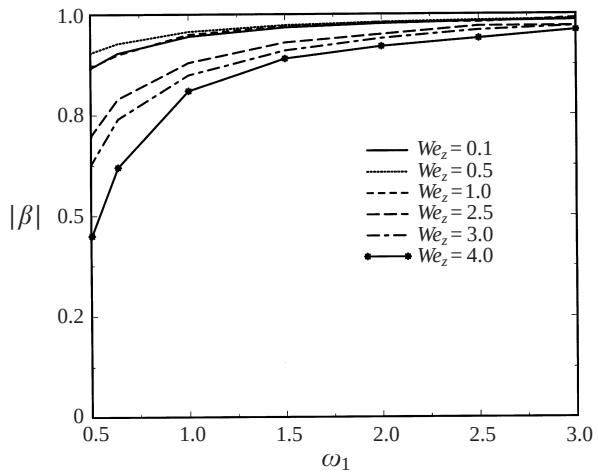

FIGURE 7. Floquet multiplier, $|\beta|$ vs. ω_1 for $\omega_1 > 0.5$. Note that $|\beta|$ asymptotes to 1 with increasing ω_1.

in figures 5 (*a*)–5 (*d*). In all cases of instability, we find that a Floquet multiplier passes through unity, so the bifurcating solutions are always periodic, with the period of the response equal to the period of the forcing: synchronous resonance. One might *a priori* expect resonant instability when $\omega_1 \approx 1/Wp$, since this is the characteristic frequency of the Hopf bifurcation that occurs in the absence of axial flow and corresponds dimensionally to the inverse relaxation time of the polymer. We do indeed observe instability in the neighbourhood of $\omega_1 = 1/Wp$, but we also find that instability can occur at frequencies much lower than $1/Wp$. Indeed at the lower values of We_z, this low-frequency region is where the largest range of wavenumbers is excited. We discuss first some typical results from the regime where instabilities at $\omega_1 \approx 1/Wp$ dominate, and then turn to the behaviour at lower frequencies.

When $We_z = 2$, instability occurs in a band of frequencies near $1/Wp$. Figure 8 shows the magnitude of the dominant Floquet multiplier, β vs. ω_1 for this value of We_z and a number of values of α. Note the increase in the magnitude of β when the

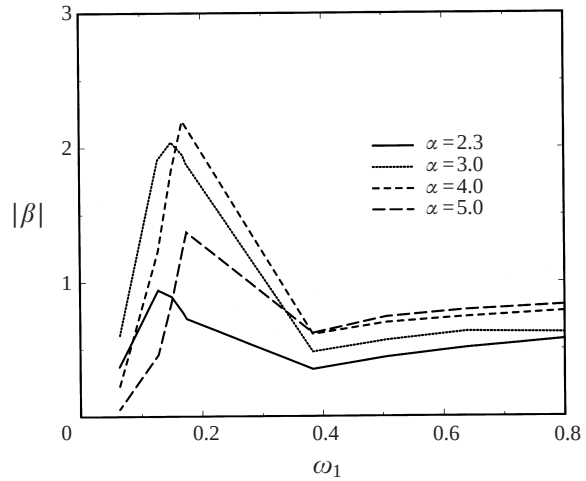

FIGURE 8. $|\beta|$ vs. ω_1 for varying α. The maximum value occurs near the inverse dimensionless relaxation time, $\omega_1 \approx 1/Wp$.

excitation frequency is near $1/Wp$ regardless of the overall stability of the system. To better illustrate the instability, we show in figures 9(*a*) and 9(*b*) the structure of $\tilde{\tau}_{\theta\theta}$ component of $\boldsymbol{\zeta}(t)$ corresponding to the dominant value of β, for $\omega_1 = 1/Wp$ (unstable) and $\omega_1 = 0.533/Wp$ (stable) respectively, with all other parameters held constant at $Wp = 5.93$, $\alpha = 4.0$, and $We_z = 2.0$. Note that for $\omega_1 = 0.533/Wp$ the variations are localized in a boundary layer near the outer cylinder while for $\omega_1 = 1/Wp$ the distribution is more uniform and approaches the radial travelling wave structure of the pure circular Couette instability.

In contrast to the behaviour when $We_z = 2$, when $We_z = 1$ there is a broad band of destabilizing frequencies, stretching from $\omega_1 \approx 1/Wp$ down to $\omega_1 = 0.005$, the lowest non-zero frequency studied. In the unstable wavenumber band, β increases dramatically as ω_1 decreases, and the calculations are no longer reliable (i.e. $\boldsymbol{\zeta}(t)$ is no longer periodic) below $\omega_1 = 0.005$. At these low frequencies, we see from figure 5(*b*) that the band of unstable wavenumbers roughly extends from 3 to 7. However, when steady axial flow is imposed, so $\omega_1 \equiv 0$, only the band from about 2 to 5 is destabilized. Clearly, the addition of periodic axial flow can have a destabilizing effect even when the corresponding steady flow is stabilizing.

The qualitative difference in the stability of the modulated and steady systems as $\omega_1 \to 0$ results is indicative of a singular limit. This has also been observed in the stabilization of Newtonian Taylor–Couette flow (Marques & Lopez 1997). The singularity of the zero frequency limit has been previously established in the literature for linear stability analysis of time-dependent flows (Rosenblat 1968; von Kerczek & Davis 1974). Davis & Rosenblat (1977) analysed a damped Mathieu–Hill equation with externally imposed modulation and showed that at low frequencies the eigenfunctions have large temporal increases in magnitude within the period of oscillation; these become unbounded as $\omega_1 \to 0$. Thus, while the Floquet analysis may predict overall stable behaviour for a suitable choice of parameters at low frequencies, the long periods of oscillation allow for large transient increases in the response. Since the perturbations in the system are now no longer infinitesimally small as is required for linear stability analysis, one would have to resort to a nonlinear theory to be able to adequately represent the solution of the system. We find that similar behaviour occurs in the CCMAC and DMAC flows. Figure 10 plots a norm of $\boldsymbol{\zeta}(t)$ vs. t/T as it

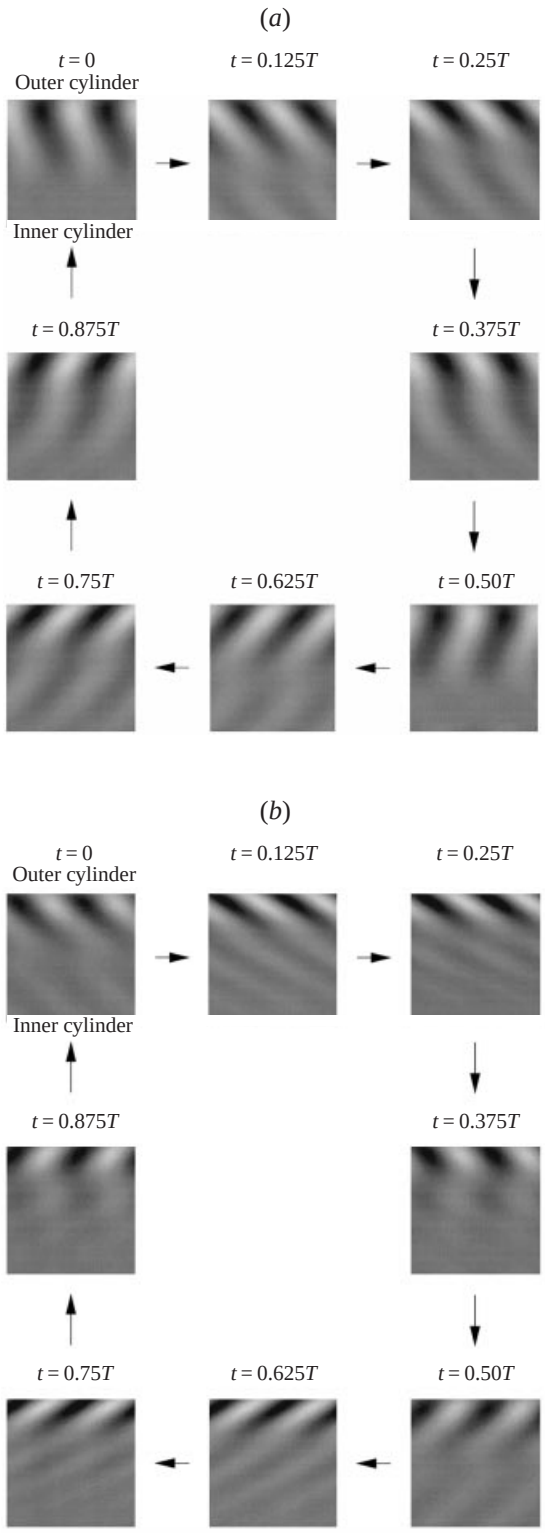

FIGURE 9. Fluctuations in the $\tilde{\tau}_{\theta\theta}$ component of $\boldsymbol{\zeta}(t)$ at $Wp = 5.93$, $We_z = 2.0$, $\alpha = 3.0$: (*a*) $\omega_1 = 1/Wp$, (*b*) $\omega_1 = 0.533/Wp$.

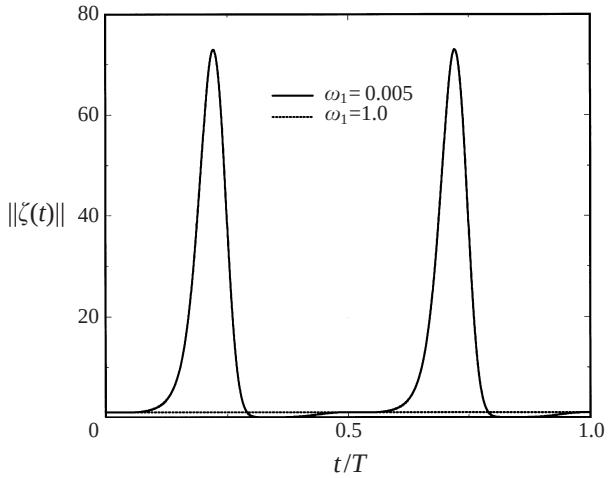

FIGURE 10. Norm of $\tilde{\tau}_{\theta\theta}$ component of $\boldsymbol{\zeta}(t)$ for $\omega_1 = 0.005$ and $\omega_1 = 1.0$ with $Wp = 5.93$, $We_z = 1.0$, and $\alpha = 4.0$.

evolves in time for $\omega_1 = 0.005$ and $\omega_1 = 1.0$ for the CCMAC case with $We_z = 1.0$ and $\alpha = 4.0$. For $\omega_1 = 0.005$, the parameter set is unstable. At approximately $t = 0.22T$ and $t = 0.72T$ there are large bursts in the perturbation amplitude for $\omega_1 = 0.005$ while for $\omega_1 = 1.0$ the amplitude is uniform in time. The increases are approximately 60 times the average magnitude outside the localized region for $\omega_1 = 0.005$ while for $\omega_1 = 1.0$ the response has no sharp increases and a maximum that is 1.02 times the initial amplitude. Figure 11 shows the fluctuations in the $\tilde{\tau}_{\theta\theta}$ component of $\boldsymbol{\zeta}(t)$ across the gap for the CCMAC flow in the neighbourhood of $t = 0.22T$. Notice that the relative magnitudes of $\boldsymbol{\zeta}(t)$ at $t = 0.156T$ and $t = 0.284T$ are negligible when compared to the disturbances at $t = 0.22T$, with spatial variations not discernible within the scale chosen in the plot. Similar trends are seen in $\boldsymbol{\zeta}(t)$ for DMAC flow at low frequencies, although destabilization does not occur. Thus, we find that the singular behaviour of $\boldsymbol{\zeta}(t)$ as $\omega \to 0$ holds regardless of whether we are in a stable region or not.

The locations of the maxima coincide with the time instants when the imposed axial velocity, given by $We_z/Wp \cos(2\pi t/T)$, goes to zero. This result would not be predicted by a quasi-steady analysis based on the results of Graham (1998). With steady axial flow, the $We_z = 0$ state is more stable than are flows with small but non-zero We_z. Thus, from quasi-steady arguments, one would predict that the disturbance amplitude would be smallest at the times when the axial shear rate, and thus the local (in time) Weissenberg number is smallest. This failure of quasi-steady arguments again underscores the singularity of the zero-frequency limit.

As a possible means to avoid the large temporal increases at low frequencies, we also investigate the effect of an axial deformation which is a sawtooth in time. This gives a velocity gradient that is a constant We_z/Wp for $0 < t \leqslant T/2$ and $-We_z/Wp$ for $T/2 < t \leqslant T$. The rationale behind this exercise is that instantaneous changes in velocity gradients might serve to damp out the large growths in the response that accompanies the slow and smooth transition in the direction of oscillation in a sinusoidally excited system at low frequencies. However, numerical calculations indicate otherwise, with stability maps showing large regions of instability for a wide spectrum of wavenumbers and frequencies investigated. It appears that the large number of harmonics present in a sawtooth deformation each tend to resonate with the applied frequency and hence lead to instability.

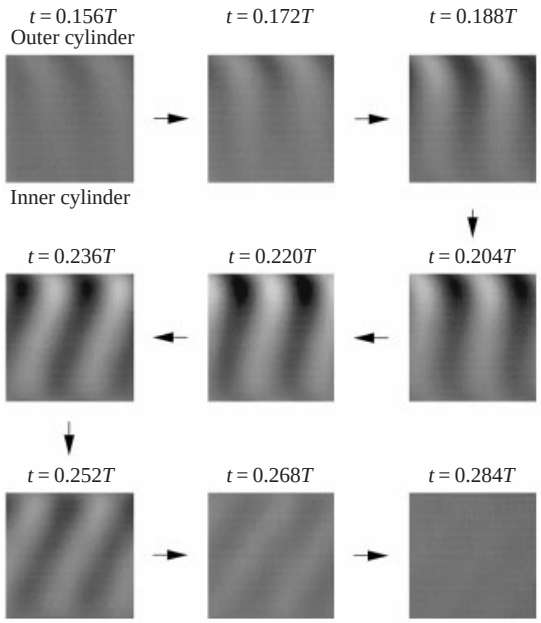

FIGURE 11. Snapshot of fluctuations in the neighbourhood of 0.22 T for CCMAC flow with $\omega_1 = 0.005$, $Wp = 5.93$, $We_z = 1.0$, and $\alpha = 4.0$.

The results presented above reflect the stability properties of the forced system relative to the critical Wp of the pure Couette and Dean flows. These results show that the axial oscillations affect stability, but not the degree of stabilization. We end with sample calculations showing how the minimum critical value of Wp is shifted by the presence of axial oscillations. For CCMAC flow, when $S = 0, \omega_1 = 0.383$, $We_z = 2.0$ we find $Wp_{c,min} = 6.4$ and $\alpha_{min} = 5.0$. Similarly, DMAC simulations for $S = 0, \omega_1 = 0.8, We_z = 2.0$ yield $Wp_{c,min} = 4.37$ and $\alpha_{min} = 6.0$. Note that in both cases we find $Wp_{c,min}$ is greater than $Wp_{c,min}$ from the pure Couette (5.93) or Dean (4.06) flows indicating increased stabilization. Again, the decrease in α_{min} with the addition of modulated flow is consistent with the analysis of Graham (1998). For comparison, the values of $Wp_{c,min}$ for $We_z = 2$ in steady axial flow would be 7.82 and 7.39 for the CCAC and DAC cases, respectively.

6. Conclusions

We have demonstrated that the superposition of axial periodic motion on the circular Couette and Dean flows can be used to delay the onset of viscoelastic instability. While the Dean flow with superposed modulated axial Couette (DMAC) flow analysis reveals that transverse motion is stabilizing for all frequencies and wavenumbers that we have investigated, the circular Couette with superimposed modulated axial Couette flow (CCMAC) system reveals distinct regimes corresponding to low and high axial Weissenberg number We_z where the flow is stabilized for all wavenumbers. Intermediate values of We_z show instability at certain wavenumbers. One interesting region of instability is when $We_z = 2$ where the instability occurs at frequencies close to the inverse of the relaxation time of the fluid. Asymptotic analysis also indicates that at high frequencies and axial Weissenberg numbers ($\omega = O(1)$, $We_z = O(\epsilon^{-1/2})$) the flow reduces to a planar shear flow that is known to be stable. This is confirmed

from our numerical results which yield stable Floquet multipliers in these regimes. Another regime of interest is when $\omega = O(1)$ and $We_z = O(1)$ where averaging theory shows that no stabilization occurs. Again, numerical computations confirm this behaviour. Further, we have examined the singularity of the $\omega \to 0$ limit, finding that the disturbances can display bursts of large magnitude separated by quiescent intervals.

We have also reported linear and weakly nonlinear stability results from the superposition of steady axial flow on Dean flow instabilities. For $We_z \gg 1$ the scaling analysis follows Graham (1998) with critical Wp varying linearly with We_z. Low We_z results in stabilization, which is qualitatively different from the circular Couette analysis of Graham (1998). Weakly nonlinear analysis reveals that the bifurcation may be subcritical or supercritical depending on the values of We_z and S. Finally, we report a codimension-2 Takens–Bogdanov bifurcation point at an axial wavenumber $\alpha = 21.9$ for Dean flow without axial forcing. This bifurcation point represents a change in the mechanism of the instability.

This work was supported by an NSF CAREER Award number CTS-9502677.

Appendix. Base-state solutions

To leading order, the steady-state velocities and polymer stresses of an Oldroyd-B fluid are given below.

DAP flow:

$$\bar{v}_r = 0, \tag{A 1}$$

$$\bar{v}_\theta = \rho(1-\rho), \tag{A 2}$$

$$\bar{v}_z = \frac{We_z}{Wp}\rho(1-\rho)\epsilon^{1/2}, \tag{A 3}$$

$$\bar{\tau}_{rr} = 0, \tag{A 4}$$

$$\bar{\tau}_{r\theta} = \frac{Wp\,(1-2\rho)}{\epsilon^{1/2}}, \tag{A 5}$$

$$\bar{\tau}_{rz} = We_z(1-2\rho), \tag{A 6}$$

$$\bar{\tau}_{\theta\theta} = \frac{2(1-2\rho)^2 Wp^2}{\epsilon}, \tag{A 7}$$

$$\bar{\tau}_{\theta z} = \frac{2(1-2\rho)^2 We_z Wp}{\epsilon^{1/2}}, \tag{A 8}$$

$$\bar{\tau}_{zz} = 2(1-2\rho)^2 We_z^2. \tag{A 9}$$

CCMAC: The equations correspond to the regime where $\omega = O(\epsilon^{1/2})$ and $t = O(\epsilon^{-1/2})$ with all other variables scaled as in §2. We define $\omega_1 = \epsilon^{-1/2}\omega = O(1)$ and $t_1 = \epsilon^{1/2}t = O(1)$.

$$\bar{v}_r = 0, \tag{A 10}$$

$$\bar{v}_\theta = (1-\rho), \tag{A 11}$$

$$\bar{v}_z = \frac{We_z(1-\rho)\epsilon^{1/2}\cos(\omega_1 t_1)}{Wp}, \tag{A 12}$$

$$\bar{\tau}_{rr} = 0, \tag{A 13}$$

$$\bar{\tau}_{r\theta} = -\frac{Wp}{\epsilon^{1/2}}, \tag{A 14}$$

$$\bar{\tau}_{rz} = -\frac{We_z \cos(\omega_1 t_1)}{(1+\omega_1^2 Wp^2)} - \frac{\omega_1 Wp\, We_z \sin(\omega_1 t_1)}{(1+\omega_1^2 Wp^2)}, \tag{A 15}$$

$$\bar{\tau}_{\theta\theta} = \frac{2Wp^2}{\epsilon}, \tag{A 16}$$

$$\bar{\tau}_{\theta z} = \frac{We_z Wp(2\cos(\omega_1 t_1) + 3Wp\,\omega_1 \sin(\omega_1 t_1) + \omega_1^3 Wp^3 \sin(\omega_1 t_1))}{\epsilon^{1/2}(1+\omega_1^2 Wp^2)^2}, \tag{A 17}$$

$$\bar{\tau}_{zz} = -\frac{-We_z^2(-1-4\omega_1^2 Wp^2 - \cos(2\omega_1 t_1) + 2\omega_1^2 Wp^2 \cos(2\omega_1 t_1) - 3\,\omega_1 Wp \sin(2\omega_1 t_1))}{(1+4\omega_1^2 Wp^2)(1+\omega_1^2 Wp^2)}. \tag{A 18}$$

DMAC: The scalings for ω and t are the same as for CCMAC. The steady axial flow (DAC) equations are obtained by setting $\omega_1 = 0$.

$$\bar{v}_r = 0, \tag{A 19}$$

$$\bar{v}_\theta = (\rho - \rho^2), \tag{A 20}$$

$$\bar{v}_z = \frac{We_z(1-\rho)\epsilon^{1/2}}{Wp}\cos(\omega_1 t), \tag{A 21}$$

$$\bar{\tau}_{rr} = 0, \tag{A 22}$$

$$\bar{\tau}_{r\theta} = \frac{Wp\,(1-2\,\rho)}{\epsilon^{1/2}}, \tag{A 23}$$

$$\bar{\tau}_{rz} = -We_z \frac{\cos(\omega_1 t_1) + Wp\,\omega_1 \sin(\omega_1 t_1)}{(1+\omega_1^2 Wp^2)}, \tag{A 24}$$

$$\bar{\tau}_{\theta\theta} = \frac{2Wp^2(1-2\rho)^2}{\epsilon}, \tag{A 25}$$

$$\bar{\tau}_{\theta z} = \frac{We_z Wp(-1+2\rho)(2\cos(\omega_1 t_1) + Wp\,\omega_1(3+Wp^2\omega_1^2)\sin(\omega_1 t_1))}{\epsilon^{1/2}(1+Wp^2\omega 1^2)^2}, \tag{A 26}$$

$$\bar{\tau}_{zz} = \frac{-We_z^2(-1-4\omega_1^2 Wp^2 - \cos(2\omega_1 t_1) + 2\omega_1^2 Wp^2\cos(2\omega_1 t_1) - 3\omega_1 Wp\sin(2\omega_1 t_1))}{(1+4Wp^2\omega_1^2)(1+Wp^2\omega_1^2)}. \tag{A 27}$$

REFERENCES

Arnoldi, W. E. 1951 The principle of minimized iteration in the solution of matrix eigenvalue problems. *Q. Appl. Maths* **9**, 17–29.

Avgousti, M. & Beris, A. N. 1993 Non-axisymmetric modes in the viscoelastic Taylor–Couette flow. *J. Non-Newtonian Fluid Mech.* **50**, 225–252.

Avgousti, M., Liu, B. & Beris, A. N. 1993 Spectral methods for the viscoelastic time-dependent flow equations with applications to Taylor–Couette flow. *Intl J. Numer. Meth. Fluids* **17**, 49–74.

Bogdanov, R. I. 1975 Versal deformations of a singular point on the plane in the case of zero eigenvalues. *Funct. Anal. Appl.* **9**, 144–145.

Canuto, C., Hussaini, M. Y., Quarteroni, A. & Zang, T. A. 1988 *Spectral Methods in Fluid Dynamics*. Springer.

Dangelmayr, G. & Knobloch, E. 1987 The Takens–Bogdanov bifurcation with $O(2)$ symmetry. *Phil. Trans. R. Soc. Lond.* A **322**, 243–279.

Davis, S. H. & Rosenblat, S. 1977 On bifurcating periodic solutions at low frequency. *Stud. Appl. Maths* **57**, 59–76.

Genieser, L. 1997 Stress and velocity field evolution in viscoelastic planar contraction flow. PhD thesis, MIT, Cambridge, MA.

Golubitsky, M., Schaeffer, D. G. & Stewart, I. 1985 *Singularities and Groups in Bifurcation Theory*, Volume 2. Springer.

Gorodtsov, V. A. & Leonov, A. I. 1967 On a linear instability of a plane parallel Couette flow of viscoelastic fluid. *J. Appl. Math. Mech.* **31**, 310–319.

Graham, M. D. 1988 Effect of axial flow on viscoelastic Taylor–Couette instability. *J. Fluid Mech.* **360**, 341–374.

Guckenheimer, J. & Knobloch, E. 1983 Nonlinear convection in a rotating layer: amplitude expansions and normal form. *Geophys. Astrophys. Fluid Dyn.* **23**, 247–272.

Hu, H. C. & Kelly, R. E. 1995 Stabilization of longitudinal vortex instabilities by means of transverse flow oscillations. *Phys. Fluids* **9**, 648–654.

Iooss, G. & Joseph, D. D. 1989 *Elementary Stability and Bifurcation Theory*. Springer.

Joo, Y. L. & Shaqfeh, E. S. G. 1991 Viscoelastic Poiseuille flow through a curved channel: a new elastic instability. *Phys. Fluids* A **3**, 1691–1694.

Joo, Y. L. & Shaqfeh, E. S. G. 1992 A purely elastic instability in Dean and Taylor–Dean flow. *Phys. Fluids* A **4**, 524–543.

Joo, Y. L. & Shaqfeh, E. S. G. 1994 Observations of purely elastic instabilities in the Taylor–Dean flow of a Boger fluid. *J. Fluid Mech.* **262**, 27–73.

Kerczek, C. von & Davis, S. H. 1974 Linear stability theory of oscillatory Stokes layers. *J. Fluid Mech.* **62**, 753–773.

Knobloch, E. & Proctor, M. R. E. 1981 Nonlinear periodic convection in double diffusive systems. *J. Fluid Mech.* **108**, 291–316.

Larson, R. G., Shaqfeh, E. S. G. & Muller, S. J. 1990 A purely elastic instability in Taylor–Couette flow. *J. Fluid Mech.* **218**, 573–600 (referred to herein as LSM).

Lehoucq, R. B., Sorensen, D. C. & Yang, C. 1997 *ARPACK Users Guide: Solutions of Large Scale Eigenvalue Problems by Implicity Restarted Arnoldi Methods.* `ftp://ftp.caam.rice.edu/pub/software/ARPACK`.

Marques, F. & Lopez, J. M. 1997 Taylor–Couette flow with axial oscillations of the inner cylinder: Floquet analysis of the basic flow. *J. Fluid Mech.* **348**, 153–176.

McKinley, G. H., Pakdel, P. & Öztekin, A. 1996 Rheological and geometric scaling of purely elastic flow instabilities. *J. Non-Newtonian Fluid Mech.* **67**, 19–47.

Northey, P. J., Armstrong, R. C. & Brown, R. A. 1992 Finite-amplitude time-periodic states in viscoelastic Taylor–Couette flow described by the UCM model. *J. Non-Newtonian Fluid Mech.* **42**, 117–139.

Olagunju, D. O. 1997 Hopf bifurcation in creeping cone-and-plate flow of a viscoelastic fluid. *Z. Angew. Math. Phys.* **48**(3), 361–369.

Rajagopalan, D., Armstrong, R. C. & Brown, R. A. 1990 Finte element methods for calculation of steady, viscoelastic flow using constitutive equations with a Newtonian viscosity. *J. Non-Newtonian Fluid Mech.* **36**, 159–192.

Renardy, M. 1997 High Weissenberg number boundary layers for the upper convected Maxwell fluid. *J. Non-Newtonian Fluid Mech.* **68**, 125–132.

Renardy, M., Renardy, Y., Sureshkumar, R. & Beris, A. N. 1996 Hopf-Hopf and steady-Hopf mode interactions in Taylor–Couette flow of an upper convected Maxwell liquid. *J. Non-Newtonian Fluid Mech.* **63**, 1–31.

Rosenblat, S. 1968 Centrifugal instability of time-dependent flows. Part 1. Inviscid, periodic flows. *J. Fluid Mech.* **33**, 321–336.

Sanders, J. A. & Verhulst, F. 1985 *Averaging Methods in Nonlinear Dynamical Systems*. Springer.

Shaqfeh, E. S. G. 1996 Purely elastic instability in viscometric flows. *Ann. Rev. Fluid Mech.* **28**, 129–185.

Shaqfeh, E. S. G., Muller, S. J. & Larson, R. G. 1992 The effects of gap width and dilute solution properties on the viscoelastic Taylor–Couette instability. *J. Fluid Mech.* **235**, 285–317.

Sureshkumar, R., Beris, A. N. & Avgousti, M. 1994 Non-axisymmetric subcritical bifurcations in viscoelastic Taylor–Couette flow. *Proc. R. Soc. Lond.* A **447**, 135–153.

Takens, F. 1974 Forced oscillations and bifurcations. In *Commun. No. 3*. Math. Inst. Rijksuniv. Utrecht, Neth.

Vermant, J., Moldenaers, P., Mewis, J., Ellis, M. & Garritano, R. 1997 Orthogonal superposition measurements using a rheometer equipped with a force rebalanced transducer. *Rev. Sci. Instrum.* **68**, 4090–4096.

Weisberg, A. Y., Kevrekidis, I. G. & Smits, A. J. 1997 Delaying transition in Taylor–Couette flow with axial motion of the inner cylinder. *J. Fluid Mech.* **348**, 141–152.